

MATE: Masked Autoencoders are Online 3D Test-Time Learners

Muhammad Jehanzeb Mirza^{†1,2} Inkyu Shin^{†3} Wei Lin^{†1} Andreas Schriebl¹
 Kunyang Sun⁴ Jaesung Choe³ Horst Possegger¹ Mateusz Kozinski¹ In So Kweon³
 Kuk-Jin Yoon³ Horst Bischof^{1,2}

¹Institute for Computer Graphics and Vision, Graz University of Technology, Austria.

²Christian Doppler Laboratory for Embedded Machine Learning.

³Korea Advanced Institute of Science and Technology (KAIST), South Korea.

⁴Southeast University, China.

Abstract

We propose MATE, the first Test-Time-Training (TTT) method designed for 3D data. It makes deep networks trained in point cloud classification robust to distribution shifts occurring in test data, which could not be anticipated during training. Like existing TTT methods, which focused on classifying 2D images in the presence of distribution shifts at test-time, MATE also leverages test data for adaptation. Its test-time objective is that of a Masked Autoencoder: Each test point cloud has a large portion of its points removed before it is fed to the network, tasked with reconstructing the full point cloud. Once the network is updated, it is used to classify the point cloud. We test MATE on several 3D object classification datasets and show that it significantly improves robustness of deep networks to several types of corruptions commonly occurring in 3D point clouds. Further, we show that MATE is very efficient in terms of the fraction of points it needs for the adaptation. It can effectively adapt given as few as 5% of tokens of each test sample, which reduces its memory footprint and makes it lightweight. We also highlight that MATE achieves competitive performance by adapting sparingly on the test data, which further reduces its computational overhead, making it ideal for real-time applications.

1. Introduction

Recent deep neural networks show impressive performance in classifying 3D point clouds. However, their success is warranted only if the test data originates from the same distribution as training data. In real-world scenarios, this assumption is often violated. A LiDAR point cloud can

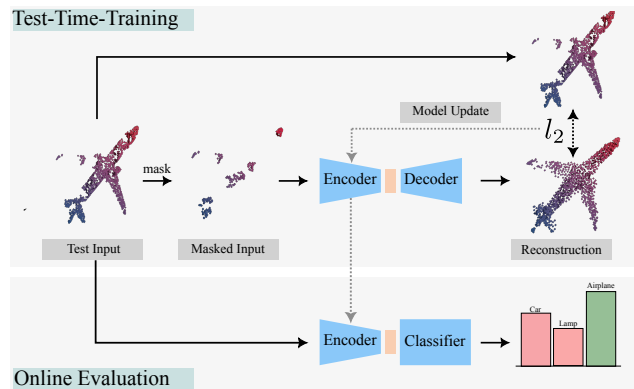


Figure 1. Overview of our Test-Time Training methodology. We adapt the encoder to a single out-of-distribution (OOD) test sample online, by updating its weights using a self-supervised reconstruction task. We then use the updated weights to make a prediction on the test sample. To enable this approach, the encoder, decoder, and the classifier were previously co-trained in the classification and reconstruction tasks [17], which is not shown in the figure.

be corrupted, for example, due to sensor malfunction, or environmental factors. It has been shown that even seemingly insignificant perturbations, like introduction of jitter or minute amount of noise to the point cloud, can significantly decrease the performance of several state of the art 3D object recognition architectures [19]. This lack of robustness can limit the utility of 3D recognition in numerous applications, including in construction industry, geo-surveying, and manufacturing. Distribution shifts that can affect 3D data are diverse in nature and it might not be feasible to train the network for all the shifts which can possibly be observed in test point clouds. Thus, there is a need to adapt to these shifts at test time, in an unsupervised manner.

[†] Equally contributing authors.

Correspondence: muhammad.mirza@icg.tugraz.at

In the domain of image classification, Test-Time-Training recently gained a lot of traction as a method to robustify classifiers to distribution shifts. It consists in using unlabeled test data to adapt the classifier to the change in data distribution. The main adaptation techniques include regularizing the classifier on test data with objective functions defined on the entropy of its predictions [13, 28, 35], updating the statistics of the batch normalization layers to match the distribution of the test data [16], and training the network on test data with self-supervised tasks [14, 25]. However, so far, none of these techniques has been applied to 3D point clouds.

In this paper, we address the problem of test-time-training for 3D point cloud classification. We adopt the self-supervised approach [14, 25], in which a deep network is adapted by training it in a self-supervised task on test data. Our choice is dictated by the availability of a self-supervised task that perfectly matches our goal of adapting 3D networks. Masked autoencoder proved very effective in pre-training 3D object recognition networks [17], and adapting deep nets to corruptions of 2D images [6]. It consists in removing a large portion of the point cloud, and tasking the network with reconstructing the entire point cloud given only the part that has not been removed. We use this procedure to update the network on every test sample that is used for the adaptation. We call our method MATE and present its overview in Figure. 1.

Our experiments on three 3D object recognition datasets show that MATE outperforms the TTT approach based on the standard rotation prediction task [25], and the feature alignment approach [16] by a large margin. Moreover, using the reconstruction task as the auxiliary objective for 3D point cloud classification has additional benefits. It makes MATE achieve significant performance gains even while masking 95% tokens of the point clouds. This seemingly a nuance can have important benefits, since at test-time the encoder only needs to process the remaining 5% of tokens to adapt the network, which radically limits the computational overhead of the adaptation. The overhead from TTT can be further reduced by adapting to test data sparingly, as MATE can achieve significant performance gains over un-adapted networks by only adapting on every 100-th sample of the ModelNet-40C [19] data set. We show that, as a result, our TTT method can reach near real-time adaptation with minimum drop in performance. Furthermore, we also find that our MATE can be successfully applied in challenging scenarios, where a stream of data is not available for adaptation, but instead test-time training needs to be performed only on a single test instance.

2. Related works

Our work is related to Unsupervised Domain Adaptation (UDA), Self-Supervised Learning (SSL) and more closely

to methods which learn on test instances.

Unsupervised Domain Adaptation. UDA methods aim to bridge the domain gap between the source and target domains without requiring access to labels from the target domain. In the image domain, Ganin *et al.* [7] propose to align features from the source and target domain with a gradient reversal layer. Similarly, CORAL [23] proposes to whiten the target domain features and then re-color them with respect to the source domain. Other methods rely on bridging the domain gap by aligning source and target features explicitly, for example through aligning higher order central moments [34]. In addition to the 2D image domain, UDA has also gained considerable traction in the 3D vision community. PointDAN [18] aligns local and global point cloud features from the source and target domain in an end-to-end manner. Yi *et al.* [32] use a sparse voxel completion network and semantic labeling for unsupervised domain adaptation for semantic segmentation. Shen *et al.* [20] first propose to encode the underlying geometry of point clouds from the target data with the help of implicit functions and resort to pseudo-labeling in the second step. For 3D object detection, adversarial augmentation is proposed by 3D-VField [20] for generalization to different domains. MLC-Net [15] propose teacher student network along with pseudo-labeling. Wang *et al.* [30] propose to bridge the domain gap for 3D object detection by using priors, such as bounding box sizes from the target domain. Although unsupervised domain adaptation approaches tackle an important problem, they assume knowledge about the test distribution and try to mitigate the effect of distribution shift by an extensive training phase. On the other hand, test-time training requires no such priors and offers a setting which is more closer to real world scenarios, where on-the-fly adaptation is required.

Self-Supervised Learning. Self-Supervised representation learning thrives on the idea of extracting supervision from the data itself. A popular SSL training objective is to bring the representations from the two randomly augmented views from the same sample closer and push apart the views from the other samples in the batch [3, 4, 12, 33]. Another approach for SSL is to extract the supervision from the reconstruction of the input data. Self-supervised representation learning by using Autoencoders [27] has been a long-standing research topic in computer vision. Recently, He *et al.* [10] revisited autoencoders and proposed Masked Autoencoders (MAE) for self-supervised representation learning in the image domain. MAE uses an asymmetric encoder-decoder structure based on ViT [5]. High proportion of the image tokens (70 – 75%) are masked and the SSL objective is to reconstruct the masked tokens. On a similar note, Pang *et al.* [17] propose Point-MAE, an MAE framework for self-supervised representation learning in 3D point cloud do-

main and show that due to the sparse nature of point clouds, a more severe masking ratio can also be employed. In our work we also use reconstruction of point clouds as an auxiliary self-supervised task for test-time training. To this end, we use the PointMAE framework and at test-time get our supervisory signal by reconstructing highly masked regions from the input point cloud.

Test-Time Adaptation. Test-Time Adaptation methods propose to add post-hoc regularization for adaptation to OOD test data. Boudiaf *et al.* [1] propose a gradient free test-time adaptation approach, which promotes consistency of output predictions coupled with Laplacian regularization. TENT [28] and MEMO [35] rely on entropy minimization from the output softmax distribution. MM-TTA [22] uses pseudo-labeling with multi-modal data for test-time adaptation. CoTTA [29] proposes student-teacher network for adaptation at test-time, while DUA [16] employs online statistical correction in the batch normalization layers for test-time adaptation. None of these techniques is demonstrated to work exclusively on 3D data. Due to its high performance and capacity of online adaptation, we selected DUA as a representative of these group of methods and adopted it to point cloud recognition. Our experiments show that MATE outperforms it by a significant margin.

Test-Time Training with Self Supervision. These methods propose to use auxiliary self-supervised tasks for adaptation to distribution shifts at test-time and are more closely linked to our MATE. Sun *et al.* [25] employ rotation prediction [8] as an auxiliary task for TTT. TTT++ [14] uses contrastive self-supervised learning (SimCLR [3]) as an auxiliary objective. A concurrent work, TTT-MAE [6] substitutes the self-supervised objective with Masked Autoencoder [10] reconstruction task for TTT in the image domain. A general insight from these works implies that the choice of auxiliary self-supervised task might be of utmost importance. MATE also employs the task of masked auto-encoding to drive the adaptation, but it reconstructs point clouds instead of images. This forces the network to encode the geometry of the point cloud and model long-range dependencies between local shapes. Furthermore, our experiments show that, for 3D point clouds, geometric reconstruction is a better auxiliary task than rotation prediction, which is employed by TTT [25] in the image domain.

3. MATE

Here, we first describe our problem setting and model architecture in detail, then we describe our training setup and finally provide details about test-time training.

3.1. Problem setting

We strictly follow the conventional test-time training setting, proposed by TTT [25]. To process the point clouds for MAE reconstruction and the downstream classification task, we use the PointMAE [17] framework. Given a point cloud $\mathcal{X} = \{\mathbf{p}_i\}_{i=1}^N$ of N points $\mathbf{p}_i = (x, y, z)^T$, the points are grouped into tokens, that is, possibly overlapping subsets of nearby points, using the farther point sampling [17]. A proportion of tokens equal to the mask ratio m is then randomly masked, yielding the masked tokens, that we denote by \mathcal{X}^m , while \mathcal{X}^v represent the remaining visible tokens. During joint training, we assume access to the training data $\mathcal{S} = \{(\mathcal{X}, \mathcal{Y})\}$, where each point cloud \mathcal{X} is accompanied by its ground truth label \mathcal{Y} . During test-time training, we do not have access to the test dataset but instead adapt to each single sample as it is encountered. After adapting the network parameters on each sample, the updated weights are used for predicting the class label. A detailed overview of different stages in our pipeline is shown in Figure 2.

3.2. Architecture

We adopt the PointMAE architecture [17], proven to work well in unsupervised pre-training for 3D object classification. It consists of an encoder E , a decoder D , a prediction head P , and a classifier head C . The encoder E is purely transformer based and receives only the unmasked point patches as input. The decoder D is similar to E , however, it is lightweight, which makes the encoder-decoder structure asymmetrical. The masked point patches and the embeddings from the unmasked point patches are fed to the decoder after concatenation. The decoder feeds the embeddings to the prediction head P , which is a simple linear fully connected layer and reconstructs the points in coordinate space. The classifier head C is a projection from the dimensions of the encoder output to the number of classes in the respective dataset. We use 3 fully connected layers with ReLU non-linearity, batch normalization and dropout as our classification head.

3.3. Joint Training

Previous methods that employ the masked autoencoder for images or point clouds [6, 17] pre-train the encoder and decoder in the self-supervised manner and subsequently train the classifier on top of it. By contrast, to make the encoder learn embeddings that at the same time describe the input geometry and are well suited for the downstream task, we train the two heads jointly. More formally, given all the parameters of the network $\{\theta_E, \theta_D, \theta_P, \theta_C\}$, the joint training is posed as

$$\min_{\theta_E, \theta_D, \theta_P, \theta_C} \mathbb{E}_{(\mathcal{X}, \mathcal{Y}) \in \mathcal{S}} [L_c(\mathcal{X}, \mathcal{Y}; \theta_E, \theta_C) + \lambda \cdot L_s(\mathcal{X}; \theta_E, \theta_D, \theta_P)], \quad (1)$$

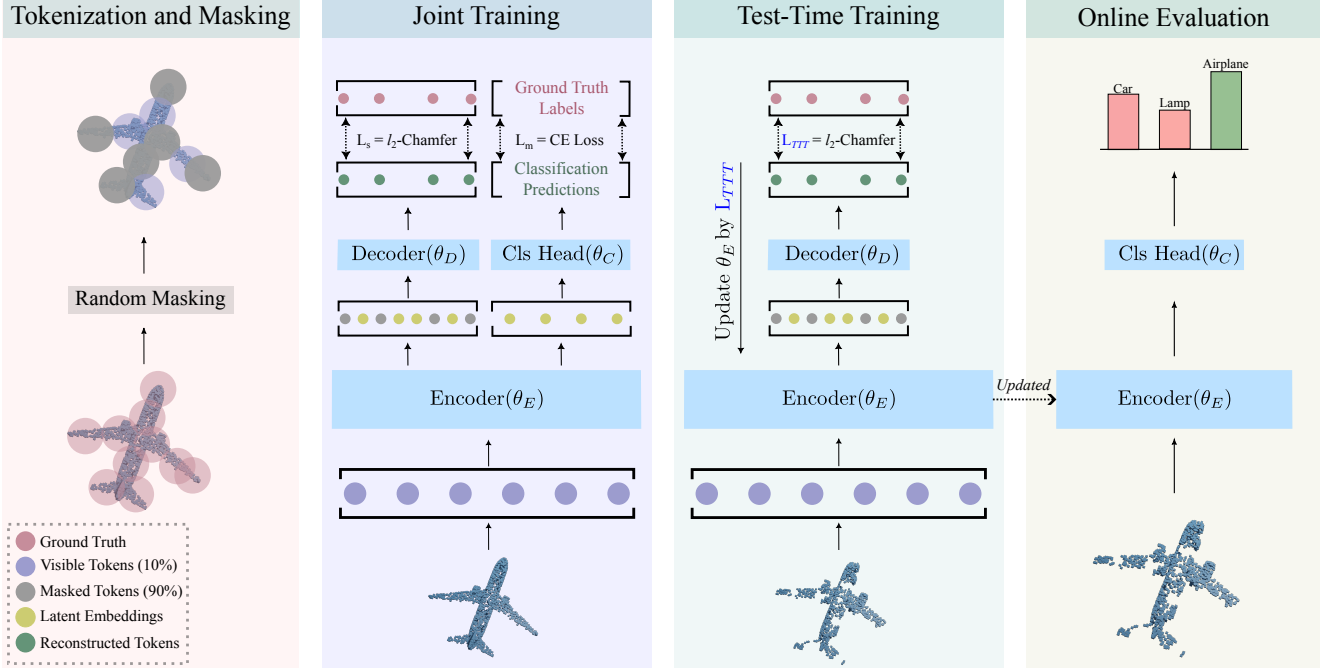


Figure 2. Overview of our 3D Test-Time Training methodology. We build on top of PointMAE. The input point cloud is first tokenized and then randomly masked. For our setup, we mask 90% of the point cloud. For joint training the visible tokens from the training data are fed to the encoder to get the latent embeddings from the visible tokens. These embeddings are fed to the classification head for the classification loss and concatenated with the masked tokens and fed to the decoder for reconstruction to obtain the reconstruction loss. Both losses are optimized jointly. For adaptation to an out-of-distribution test sample at test-time, we only use the MAE reconstruction task. Finally, after adapting the encoder on this single sample, evaluation is performed by using the updated encoder weights.

where the expectation is taken over the training set \mathcal{S} , and the hyper-parameter λ balances the two tasks. We set $\lambda = 1$ for all experiments. Here, L_c is a cross entropy (CE) loss to learn the main classification task

$$L_c(\mathcal{X}, \mathcal{Y}; \theta_E, \theta_C) = CE(C \circ E(\mathcal{X}^v), \mathcal{Y}), \quad (2)$$

where \mathcal{X}^v are the visible tokens and L_s is the self-supervised loss. Following [17], we use

$$L_s(\mathcal{X}; \theta_E, \theta_D, \theta_P) = CD(P \circ D \circ E(\mathcal{X}^v), \mathcal{X}), \quad (3)$$

which is the Chamfer distance CD between the reconstructed tokens, and the training point sets \mathcal{X} .

3.4. Test-Time Training

Given the parameters $\{\theta_E, \theta_D, \theta_P, \theta_C\}$, trained jointly for the main classification task and the self-supervised reconstruction task on the training data until convergence, our goal at test-time is to adapt to the out-of-distribution test data in an unsupervised manner, to achieve generalization. For this purpose we use the self-supervised MAE reconstruction task to adapt the network parameters to the out-of-distribution test sample.

For adaptation at test-time, we are granted access to only a single out-of-distribution point-cloud $\tilde{\mathcal{X}}$, without any ground

truth label. The point cloud is tokenized and masked, and processed by the encoder E which yields the encoding vector. Finally, the patch encodings and the masked patches are concatenated and fed to the decoder D and ultimately to the prediction head P to obtain the reconstructed point cloud. The reconstruction loss is again an l_2 Chamfer distance between the reconstructed masked tokens and the corresponding ground truth tokens from the original out-of-distribution (OOD) test sample. Our objective at test-time is to update the parameters of the encoder θ_E , decoder θ_D and the prediction head θ_P to generalize to the OOD test sample. More formally, we minimize

$$L_{TTT} = \min_{\theta_E, \theta_D, \theta_P} L_s(\tilde{\mathcal{X}}; \theta_E, \theta_D, \theta_P). \quad (4)$$

Although for the downstream task of object classification, we only require the updated encoder, through experiments we find that updating the parameters of the decoder and the prediction head have no effect on the final classification performance.

3.5. Online Adaptation Variants

After adapting the encoder weights by the reconstruction loss during test-time training, prediction scores for the OOD

sample are obtained by using the classifier head C , from the joint training phase. Following TTT [25], we provide two versions of our MATE, which are described as follows:

MATE-Standard only assumes access to a single point cloud sample at test time and the goal is to iteratively adjust the weights on the single sample in order to make the right prediction. For this purpose, we perform 20 gradient steps on the encoder parameters θ_E to minimize the objective (4), computed for one test sample. As the next sample is received, we reinitialize the weights for all the parameters $\{\theta_E, \theta_D, \theta_P\}$ and repeat the same process again.

MATE-Online assumes that point clouds are received in a stream. For this version, we accumulate the model updates after adaptation on each sample. We only calculate (and backpropagate) through (4) once for each sample.

3.6. Augmentations

During joint-training we only train the network with point cloud scale and translate augmentations, as originally used by the authors of PointMAE. For test-time training we do not use any augmentation, instead we construct a batch from the single point cloud sample and for Masked Autoencoder reconstruction, we randomly mask 90% of the tokens. Random masking is essential for MAE and also provides us with a natural augmentation. We further find that we can increase the masking ratio up to 95% and still get an impressive performance improvement. This is in contrast to images where a masking ratio of up to 70–75% is employed. Higher masking ratios helps in efficient test-time training, since only the unmasked tokens are processed by the encoder, which carries the majority of the computation effort because it has a larger structure than the decoder.

4. Experimental Evaluation

We provide results for both the Standard and the Online evaluation protocols. Here, we first describe the datasets we use for evaluation, second we provide our implementation details and later present our results.

4.1. Datasets

We test MATE on the task of object classification for 3D point clouds. To this end, we use 3 popular object classification datasets.

ModelNet-40C. ModelNet-40C [9, 24] is a benchmark for evaluating robustness of point cloud classification architectures. In this benchmark, 15 common types of corruptions are induced on the original test set of ModelNet-40 [31]. These corruptions are divided into 3 parent categories comprising *transformation*, *noise* and *density*. Their goal is to

mimic distribution shifts which occur in real-world, *e.g.*, common noise patterns on a LiDAR scan due to fault in the sensors capturing the data.

ShapeNet-C. ShapeNetCore-v2 [2] is a large-scale point cloud classification dataset consisting of 51127 shapes from 55 categories. We divide this dataset into three splits, train (35789, 70%), validation (5113, 10%) and test (10225, 20%). We provoke 15 different corruptions in the test set of ShapeNet, similar to ModelNet-40C, by using the open source implementation provided by [24]. We refer to this dataset as ShapeNet-C.

ScanObjectNN-C. ScanObjectNN [26] is a point cloud classification dataset which is collected in the real-world. It consists of 15 categories with 2309 samples in the train set and 581 samples in the test set. We again use the open source code provided by [24] to cause 15 different corruptions in the test set of ScanObjectNN for our evaluations, which we refer to as ScanObjectNN-C.

4.2. Implementation Details

We jointly train a network for supervised classification and self-supervised reconstruction tasks, as described in Sec. 3.3. We use the MAE reconstruction task as our auxiliary objective and for this purpose we build upon the point-based masked autoencoder [17] framework. For joint training, we add a classifier head which takes the feature embeddings from the encoder of the PointMAE and outputs the prediction scores. The classifier head consists of 3 linear layers with Batch Normalization, ReLU non-linearity and dropout. This is the same classification head used by PointMAE during the finetuning step. For joint training we only use 10% of the visible tokens for the self-supervised reconstruction and the classification task. However, to obtain the final classification scores at test time, we always feed 100% of the tokens to the PointMAE backbone. For ModelNet-40 and ShapeNetCore experiments, we train the networks from scratch for 300 epochs with a learning rate of 0.001 and Cosine scheduler. ScanObjectNN is a small-scale dataset, thus, we finetune the PointMAE network pre-trained on the large-scale ShapeNet-55 [2] dataset with a learning rate of 0.0005 and a Cosine scheduler for only 100 epochs, to avoid overfitting. All these models are trained by using only the point cloud scale and translate augmentation. Note that these are also the only augmentations used by the PointMAE paper¹.

During test-time training we update the encoder, decoder and the prediction head only. The classification head remains frozen. We use a learning rate of $5e - 5$ for TTT on

¹We avoid other augmentations, *e.g.* jitter or rotation, because they might correlate with the corruptions in the ModelNet-C benchmark and can provide us with an unfair advantage during TTT.

	corruptions: uni gauss backg impul upsam rbf rbf-inv den-dec dens-inc shear rot cut distort oclslion lidar Mean															
Source-Only	66.6	59.2	7.2	31.7	74.6	67.7	69.7	59.3	75.1	74.4	38.1	53.7	70.0	38.6	23.4	53.9
Joint-Training	62.4	57.0	32.0	58.8	72.1	61.4	64.2	75.1	80.8	67.6	31.3	70.4	64.8	36.2	29.1	57.6
DUA	65.0	58.5	14.7	48.5	68.8	62.8	63.2	62.1	66.2	68.8	<u>46.2</u>	53.8	64.7	<u>41.2</u>	<u>36.5</u>	54.7
TTT-Rot	61.3	58.3	34.5	48.9	66.7	63.6	63.9	59.8	68.6	55.2	27.3	54.6	64.0	40.0	29.1	53.0
MATE-Standard	<u>75.0</u>	<u>71.1</u>	27.5	<u>67.5</u>	<u>78.7</u>	<u>69.5</u>	<u>72.0</u>	79.1	84.5	<u>75.4</u>	44.4	<u>73.6</u>	<u>72.9</u>	39.7	34.2	<u>64.3</u>
MATE-Online	82.9	80.6	<u>32.4</u>	74.0	85.7	78.3	80.2	<u>78.1</u>	86.5	79.3	56.6	77.9	77.1	49.7	50.0	71.3

Table 1. Top-1 Classification Accuracy (%) for all distribution shifts in the ModelNet-40C dataset. All results are for the PointMAE backbone trained on clean train set. *Source-Only* denotes its performance on the corrupted test data without any adaptation. Highest Accuracy is shown in bold, while second best is underlined.

	corruptions: uni gauss backg impul upsam rbf rbf-inv den-dec dens-inc shear rot cut distort oclslion lidar Mean															
Source-Only	69.2	62.8	10.3	56.2	70.1	70.5	71.9	<u>85.5</u>	<u>86.2</u>	73.9	41.3	<u>84.4</u>	69.9	7.9	3.9	57.6
Joint-Training	72.5	66.4	15.0	60.6	72.8	72.6	73.4	85.2	85.8	74.1	42.8	84.3	71.7	8.4	4.3	59.3
DUA	76.1	70.1	14.3	60.9	76.2	71.6	72.9	80.0	83.8	77.1	<u>57.5</u>	75.0	72.1	11.9	12.1	60.8
TTT-Rot	74.6	72.4	<u>23.1</u>	59.9	74.9	73.8	75.0	81.4	82.0	69.2	49.1	79.9	72.7	<u>14.0</u>	12.0	60.9
MATE-Standard	<u>77.8</u>	<u>74.7</u>	4.3	<u>66.2</u>	<u>78.6</u>	<u>76.3</u>	<u>75.3</u>	86.1	86.6	<u>79.2</u>	56.1	84.1	<u>76.1</u>	12.3	<u>13.1</u>	<u>63.1</u>
MATE-Online	81.5	78.6	40.9	75.9	81.6	79.7	80.1	84.9	85.9	81.8	70.8	85.1	79.0	14.2	16.6	69.1

Table 2. Top-1 Classification Accuracy (%) for all distribution shifts in the ShapeNet-C dataset. All results are for the PointMAE backbone trained on clean train set. *Source-Only* denotes its performance on the corrupted test data without any adaptation. Highest Accuracy is shown in bold, while second best is underlined.

Method	Accuracy (%)	Method	Accuracy (%)
Source	45.7	TTT-Rot	46.1
JT	45.6	MATE-S	47.0
DUA	46.0	MATE-O	48.5

Table 3. Mean Top-1 Classification Accuracy (%) averaged over the 15 corruptions in the ScanObjectNN-C dataset. JT: Joint Training, MATE-S: MATE-Standard, MATE-O: MATE-Online

ModelNet-40C, a learning rate of $1e - 4$ for ShapeNet-C and ScanObjectNN-C. We use AdamW optimizer for both, pre-training and the test-time training. To calculate the test-time training loss, we construct a batch of 48 from the single corrupted point cloud at test-time and randomly mask 90% of each sample in the batch.

4.3. Baselines

We compare our MATE to other TTT approaches, which assume access to only a single test sample for adaptation at test-time. To this end, we adapt 2 baselines designed for image classification, since MATE is the first paper for 3D TTT. The complete set of our baselines is as follows.

- *Source Only* refers to the PointMAE backbone trained in a supervised manner on the classification task only. We use the encoder outputs and feed them to the classifier head of the PointMAE. For these results, we do not mask the tokens, instead feed the entire point cloud for training and

classification.

- *Joint Training* [11] results are obtained by training the network jointly on the classification and MAE reconstruction task and testing it on the target data (*e.g.* ModelNet-40C) without adaptation. In the image domain it is shown that Joint Training helps to make the network more robust to out-of-distribution data.

- *DUA* [16] updates the batch normalization statistics to adapt to out-of-distribution test images at test-time. We implement DUA for test-time training on point clouds and use the settings which the authors propose in the paper. DUA also makes a batch out of a single sample at test-time for adaptation. We fix this batch size to 48 for a fair comparison with MATE.

- *TTT-Rot* [25] with self-supervised rotation prediction task proposes to adapt to test data at test-time by predicting the rotation of images. We use the settings proposed in the original paper and train the network jointly for the rotation prediction task and the supervised classification task by using 100% of tokens from the input point cloud. For adaptation at test time we make a batch of 48 and adapt the network with the auxiliary loss.

4.4. Results

ModelNet-40C: In Table 1 we provide the results for all the distribution shifts in the ModelNet-40C dataset. From the table, we see that our MATE outperforms other baselines comfortably. Furthermore, even our MATE-Standard out-

	Mask Ratio (%)					
	97.5	95	90	80	70	60
MATE Online	56.9	71.6	71.3	71.5	71.6	71.5

Table 4. Mean Top-1 Classification Accuracy (%) over all corruptions in the ModelNet-40C dataset, while using different masking ratios for test-time training. The accuracy for Source-Only baseline is 57.6%.

performs the baselines with a considerable margin and we also perform favorably on individual distribution shifts. The mean performance over all corruptions of TTT-Rot falls below Source-Only, this could be an indication that the rotation prediction task is not well suited for test-time adaptation. However, for Background corruption TTT-Rot [25] fares well. This might be because Background corruption introduces artifacts in the background and TTT-Rot uses the entire point cloud for test-time adaptation, so it can adapt to this corruption better. On the other hand, we only adapt with 10% of the visible tokens and might not be able to capture these artifacts introduced in the background. Furthermore, we analyze the reconstructions from the background corruption and find that the reconstruction results are worse as compared to other corruptions. We add these results in the supplemental. These reconstruction results suggest that the reconstruction task is co-related with the classification task. Hence, better reconstruction accounts for better adaptation performance. We also see a similar trend for the TTT loss and classification accuracy at each adaptation step for corruptions in the ModelNet-40C. These results are also delegated to the supplemental.

ShapeNet-C: In Table 2 we provide Top-1 Accuracy (%) for object classification on the ShapeNet-C dataset. We again see that both evaluation protocols of our MATE show impressive results on the large-scale ShapeNet dataset. MATE-Online has a huge performance gain over other baselines, which is expected, since for these evaluations we accumulate the model updates. Similarly, MATE-Standard also outperforms other baselines and even surpasses MATE-Online on the density-related corruptions of the point clouds.

ScanObjectNN-C: We also test our MATE on point clouds collected in real world, on which we introduce the corruptions proposed in the ModelNet-C benchmark [24]. The results are provided in Table 3. On this dataset our results also show a consistent improvement over the baselines. These results show the applicability of MATE on data collected in the real world scenarios as well.

	Batch Size for Test-Time Training							
	1	2	8	16	24	32	40	48
MATE Online	43.1	66.4	69.7	70.2	70.4	70.5	70.5	71.3

Table 5. The effect of batch size for TTT. We provide the Mean Top-1 Accuracy (%) over all the corruptions in the ModelNet-40C dataset for different batch sizes. The accuracy for Source-Only baseline is 57.6%.

5. Ablation Studies

We additionally test how MATE performs with different masking ratios, scenarios where sparing adaptation on test samples is required, the effect of batch size on TTT and the effect on performance while combining multiple corruption types together.

5.1. Masking Ratios

The PointMAE has an asymmetric encoder-decoder design. The decoder is a lightweight architecture, while the encoder is a deeper network. Therefore, most of the computation effort is spent in the encoding part of the pipeline. Since the encoder processes only the visible tokens, higher masking ratio implies lower burden for the encoder. We find that our MATE can work with extremely high masking ratios, making test-time training very efficient. The results for adaptation with different masking ratios are provided in Table 4. We see that even with a severe masking of 95% of the tokens (*i.e.* only processing 5% visible tokens), our MATE can achieve 14 percent-points over the Source-Only (without adaptation) results. With 97.5% masking, we still improve on the Source-Only results. These results also show that lower masking ratios do not give us more gain in performance but instead could induce latency during test-time adaptation.

5.2. Strides for TTT

Some applications might require adaptation at test-time with minimum latency. For example, a test-time training method deployed in autonomous vehicles would ideally be required to adapt at a high frame-rate per second (FPS). Thus, a test-time training method should ideally be able to run with *close to real-time* adaptation speed. Since most of the computation overhead for adaptation methods is during the backward pass, adapting to test samples sparingly should help to reduce the computation effort. In order to scratch the boundaries of our MATE for achieving a higher FPS, we design an experiment where we only adapt at test-time after a certain number of samples (stride). Results for ShapeNet dataset in this scenario are provided in Figure 3. When performing an adaptation step after a stride, we find that our

	Source	JT	DUA	TTT-Rot	MATE-S	MATE-O
Comb - 1	33.9	36.7	42.6	34.3	47.7	55.7
Comb - 2	29.6	34.7	40.6	32.9	45.2	51.4
Comb - 3	28.3	33.3	41.5	30.7	44.5	52.5
Mean	30.6	34.8	41.6	32.6	45.8	53.2

Table 6. Top-1 Mean Accuracy (%) for three different datasets constructed by combining 2 randomly chosen corruptions for each subsequent sample in the test-set of ModelNet-40. JT: Joint Training, MATE-S: MATE-Standard, MATE-O: MATE-Online

MATE can achieve close to real-time performance, with a minimum performance penalty. For example, when we take a gradient step on every 5-th sample, MATE can achieve an FPS² up to 20 (for reference 30 FPS is often considered as real-time [21]) with only ~ 3 percent-point drop in performance while comparing with the results obtained with a stride of 1 (adapting on each incoming sample). We can even increase the stride up to 300 and still achieve ~ 3 percent point better performance than the Source-Only results, with an FPS of 62. These results indicate the efficient nature of our MATE and its ability to show effective real-time adaptation performance. We also test MATE on ModelNet-40C in this experimental protocol. These results are provided in the supplemental.

5.3. Batch Size for Test-Time Training

MATE constructs a batch of 48 from each point cloud encountered at test-time for adaptation. The point cloud in this batch is randomly masked and then masked patches are reconstructed. Random masking helps us achieve a natural augmentation during test-time training. To test the effect of our design choice on the test-time training performance, we experiment with different batch sizes on the ModelNet-40C dataset. These results are provided in Table 5. Surprisingly, for batch size of 1, test-time adaptation performance falls below Source-Only but is 8.8 percent-point better than Source-Only for the batch size of 2. We also see that batch size larger than 8 achieve minor gains, thus it could be a resource-efficient alternative.

5.4. Combination of Distribution Shifts

In realistic scenarios there could be situations where the test sample might be corrupted with a combination of corruptions. Thus, a test-time training method should be able to cope with such scenarios as well. To test our MATE in such a scenario, we design an experiment where we randomly combine 2 corruption types (from the ModelNet-40C benchmark) for each sample in the test set of ModelNet-40 and create 3 such datasets. To generate these datasets, we ensure

²The calculation of FPS is hardware specific. For reference, we run these experiments on an NVIDIA® GeForce® RTX 3090.

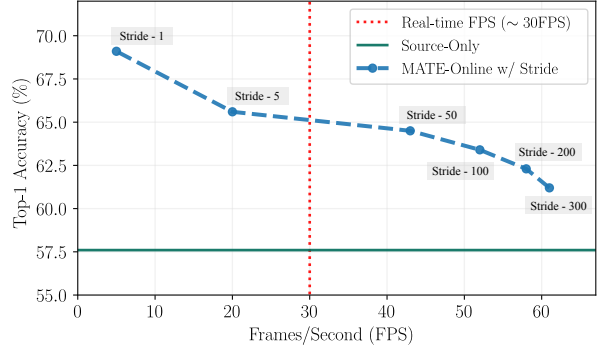


Figure 3. MATE can achieve real-time adaptation performance by only sacrificing some percent-points. Here, we report the Mean Top-1 Accuracy (%) over the 15 corruptions in the ShapeNet-C dataset for different adaptation strides. Strides represent the number of samples after which an adaptation step is performed.

that all 15 corruption types are selected for each dataset and for each sample 2 corruptions are chosen randomly from the set of 15 corruptions. We test our MATE and other baselines on these datasets and provide the results in Table 6. We see that MATE can effectively adapt to this scenario as well and outperforms other baselines by a considerable margin. DUA fares better than TTT-Rot, which is another indication that rotation prediction might not be a suitable test-time training objective for 3D point clouds.

6. Conclusion

Test-time training has been extensively studied for the image domain, however, to the best of our knowledge it has not yet been explored for the 3D point clouds. We are the first to propose an online test-time training method exclusively for 3D point clouds by using self-supervised reconstruction task as an auxiliary objective to adapt to each OOD sample encountered at test-time. Through our experiments we find that masked auto encoder is a powerful self-supervised auxiliary objective, which can make the network robust to various kinds of distribution shifts occurring in 3D point clouds. Our test-time training method, MATE, also shows important properties like adapting to multiple distribution shifts and real-time adaptation at test-time.

Supplementary material

A. Real-time Test-time Training

In the main manuscript (Figure 3), we provide results for MATE-Online while adapting sparingly to the test samples in ShapeNet-C dataset. We see that, while adapting sparingly on the test data, *i.e.* only back-propagating gradients after a certain number of samples (stride), our MATE can still achieve strong performance gains and can even match the real-time FPS (30), with only a minimum penalty on accuracy. Here, in Figure 4, we provide the results with different strides for the ModelNet-40C dataset, which is $\sim 4\times$ smaller than the ShapeNet-C dataset. While adapting sparingly, we see that, similar to the results on the large-scale ShapeNet-C, our MATE can also achieve close to *real-time* performance by dropping only a few percent-points as compared to adapting on each sample. For example, with a stride of 5 (adapting on every 5-th sample), our MATE drops only ~ 3 percent-points as compared to the results with stride-1 (adapting on each incoming sample), while obtaining an FPS of 21.

B. Classification and Reconstruction

At test-time, MATE adapts to each out-of-distribution (OOD) test sample by using the self-supervised reconstruction task as an auxiliary objective, leveraging masked autoencoders [17]. As each OOD sample is encountered, the network is adapted by the auxiliary self-supervised loss. This loss is an l_2 Chamfer distance between the reconstructed masked tokens and the corresponding ground truth tokens from the original OOD test sample. After adapting the network by back-propagating the gradients obtained from the auxiliary loss, the OOD sample is evaluated. In the main manuscript we see that our test-time training methodology achieves strong performance gains on a variety of datasets for object classification in 3D point clouds.

Naturally, the question arises – ‘How a self-supervised task, *i.e.* reconstruction task, can help to adapt the network for a seemingly un-related task, like object classification?’ Through our experiments we find that there is a correlation between the reconstruction task and the classification task and that is the reason for the improvement in classification accuracy by simply reconstructing the corrupted (OOD) test sample at test-time. We find this correlation empirically through two procedures, detailed in the following.

B.1. Loss and Accuracy

In the main manuscript, we test our MATE in two test-time training variants, described in Section 3.5, here we again provide a brief description in interest of keeping the reading flow:

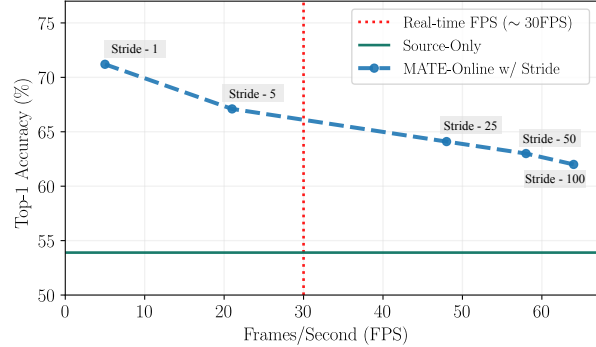


Figure 4. MATE can achieve real-time adaptation performance by only sacrificing some percent-points. Here, we report the Mean Top-1 Accuracy (%) over the 15 corruptions in the ModelNet-40C dataset for different adaptation strides. Strides represent the number of samples after which an adaptation step is performed.

MATE-Standard assumes access to a single sample at test-time for adaptation. In order to adapt the network on this single sample, we take multiple gradient steps (*i.e.* 20) for test-time training. After adaptation on each sample, the network weights are re-initialized for adaptation on the next sample.

MATE-Online assumes access to a stream of data for adaptation and the network updates are accumulated after adaptation on each sample in the stream. For this adaptation variant, we only take a single gradient step on each OOD test sample.

In Figure 5 we plot the Top-1 Accuracy on ModelNet-40C and the corresponding reconstruction loss at each gradient step for MATE-Standard. Please note that these results are plotted by taking the average of the accuracy over all the samples in the test set of ModelNet-40C at each gradient step. From the results it is evident that as the reconstruction loss decreases after each gradient step, the corresponding accuracy increases. This shows that as the model becomes better at reconstructing the OOD test sample, the classification performance is influenced in a positive way. We also see that there is a spike in the reconstruction loss during the initial update step. We hypothesize that this is because of the sudden distribution shift which is encountered at test-time, since the model is initially trained on clean point clouds. However, with more adaptation steps for test-time training, it slowly gets better at reconstructing the OOD sample.

Furthermore, an interesting result is that of the *Background* corruption. In the main manuscript, while listing the results for ModelNet-C (Section 4.4) we found that for the background corruption TTT-Rot [25] fares better than our MATE. From Figure 5, we see that for Background corruption the reconstruction loss is highest among all the other

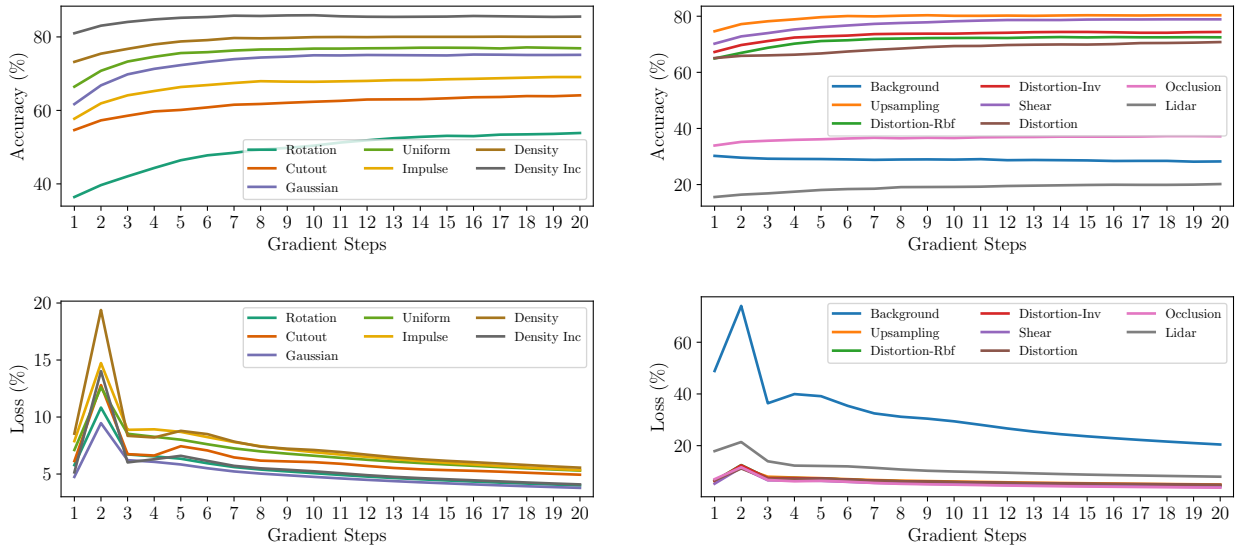


Figure 5. Accuracy (Top) and Reconstruction Loss (Bottom) for all corruption in the ModelNet-40C at each adaptation step for MATE-Standard. To avoid clutter, we split the different corruptions into two plots (left and right).

corruptions, that can be one of the reasons why MATE cannot perform well on this corruption. This also gives us an indication of the correlation between the reconstruction and the classification loss. To further investigate the background corruption and find more answers behind correlation of the two tasks, we visualize the reconstruction results next.

B.2. Reconstruction Results

We further analyzed the reconstruction results for different corruption types to get a deeper insight in to the correlation of the MAE reconstruction and the classification task. We find that for TTT with MATE-Standard, after 20 gradient steps, the reconstruction for the Background corruption is the worst as compared to reconstruction of other corruption types. We visualize these results for a few corruptions in the ModelNet-40C dataset for the *Airplane* class in Figure 6. Reconstructions from the remaining corruptions also follow a similar pattern. Since MATE does not perform optimally for the Background corruption, this gives us an indication of the correlation between the auxiliary self-supervised reconstruction task and the downstream classification task. To conclude, our results show that if the auxiliary self-supervised reconstruction task is able to reconstruct the input corruption type optimally, MATE shows strong performance gains, which is an indication that these two tasks are correlated with each other.

C. Limitation

As we adapt to each test sample at test-time before evaluation, our method can put an overhead and is generally slower

than a source model tasked only with inference. Although we can achieve a speedup with a minimum performance penalty by adapting sparingly, however, latency might be a limiting factor for application in real-time systems.

Through our experiments we find that reconstruction of aggressively masked inputs can provide us with an effective self-supervised signal to adapt the network to OOD test sample at test-time for the object classification scenario in 3D point clouds. However, there are currently no guarantees that reconstruction task can provide a useful adaptation signal for other downstream tasks. We leave it for future exploration.

References

- [1] Malik Boudiaf, Romain Mueller, Ismail Ben Ayed, and Luca Bertinetto. Parameter-free Online Test-time Adaptation. In *Proc. CVPR*, 2022. 3
- [2] Angel X Chang, Thomas Funkhouser, Leonidas Guibas, Pat Hanrahan, Qixing Huang, Zimo Li, Silvio Savarese, Manolis Savva, Shuran Song, Hao Su, et al. ShapeNet: An Information-Rich 3D Model Repository. *arXiv preprint arXiv:1512.03012*, 2015. 5
- [3] Ting Chen, Simon Kornblith, Mohammad Norouzi, and Geoffrey Hinton. A Simple Framework for Contrastive Learning of Visual Representations. In *Proc. ICML*, 2020. 2, 3
- [4] Xinlei Chen and Kaiming He. Exploring Simple Siamese Representation Learning. In *Proc. CVPR*, 2021. 2
- [5] Alexey Dosovitskiy, Lucas Beyer, Alexander Kolesnikov, Dirk Weissenborn, Xiaohua Zhai, Thomas Unterthiner, Mostafa Dehghani, Matthias Minderer, Georg Heigold, Sylvain Gelly, et al. An Image is Worth 16x16 Words: Trans-

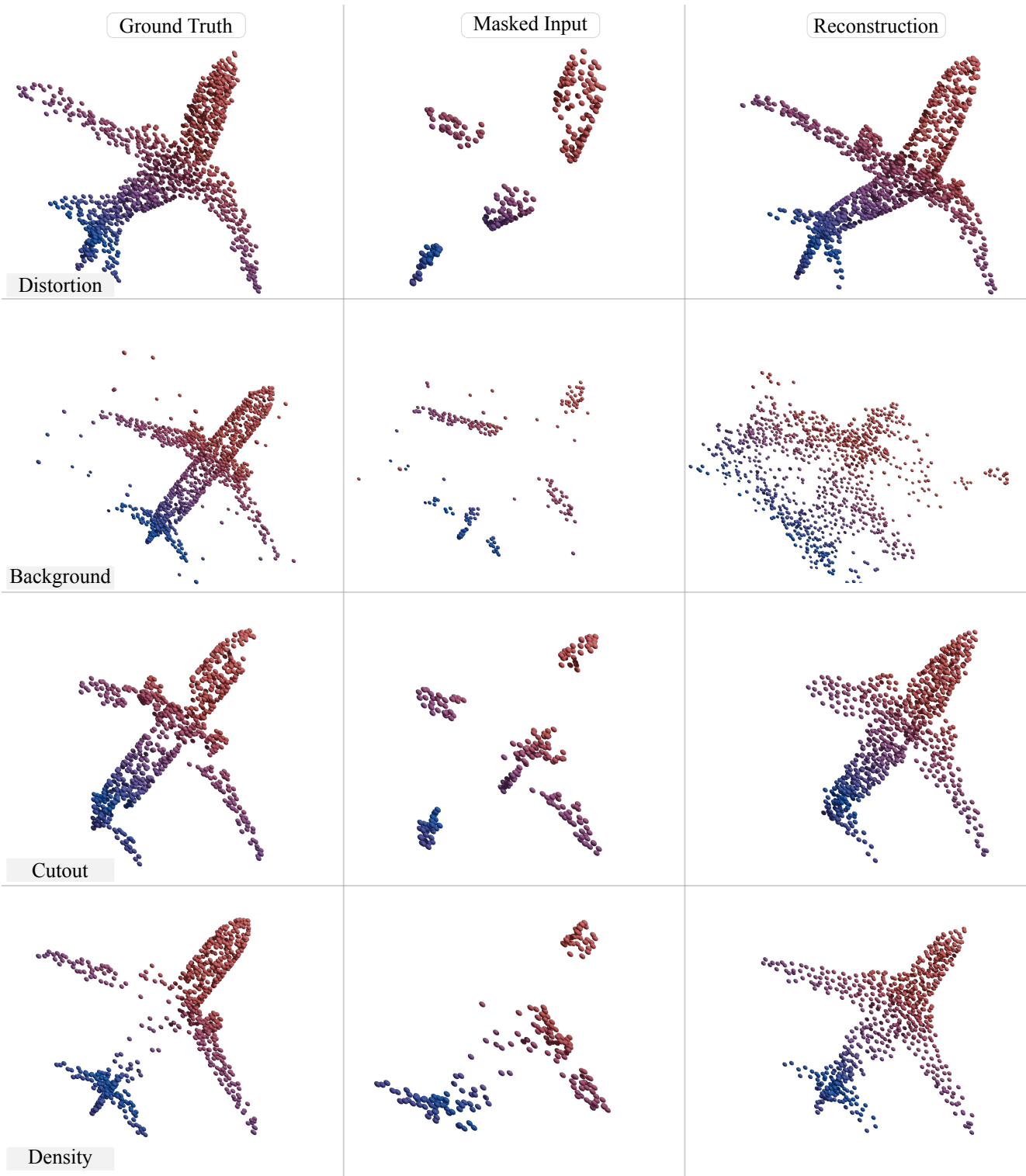


Figure 6. Reconstruction results for MATE-Standard at the 20-th gradient step for adaptation at test-time. We plot the out-of-distribution test sample for adaptation (left), 10% input visible tokens (center) and the corresponding reconstruction output (right) for four corruptions in the ModelNet-40C dataset.

- formers for Image Recognition at Scale. *arXiv preprint arXiv:2010.11929*, 2020. 2
- [6] Yossi Gandelsman, Yu Sun, Xinlei Chen, and Alexei A Efros. Test-Time Training with Masked Autoencoders. *arXiv preprint arXiv:2209.07522*, 2022. 2, 3
- [7] Yaroslav Ganin, Evgeniya Ustinova, Hana Ajakan, Pascal Germain, Hugo Larochelle, François Laviolette, Mario Marchand, and Victor Lempitsky. Domain-Adversarial Training of Neural Networks. *JMLR*, 2016. 2
- [8] Spyros Gidaris, Praveer Singh, and Nikos Komodakis. Unsupervised Representation Learning by Predicting Image Rotations. In *Proc. ICLR*, 2018. 3
- [9] Ankit Goyal, Hei Law, Bowei Liu, Alejandro Newell, and Jia Deng. Revisiting Point Cloud Shape Classification with a Simple and Effective Baseline. In *Proc. ICML*, 2021. 5
- [10] Kaiming He, Xinlei Chen, Saining Xie, Yanghao Li, Piotr Dollár, and Ross Girshick. Masked Autoencoders Are Scalable Vision Learners. In *Proc. CVPR*, 2022. 2, 3
- [11] Dan Hendrycks, Kimin Lee, and Mantas Mazeika. Using Pre-Training Can Improve Model Robustness and Uncertainty. In *Proc. ICML*, 2019. 6
- [12] Siyuan Huang, Yichen Xie, Song-Chun Zhu, and Yixin Zhu. Spatio-temporal Self-Supervised Representation Learning for 3D Point Clouds. In *Proc. CVPR*, 2021. 2
- [13] J. Liang et al. Do We Really Need to Access the Source Data? Source Hypothesis Transfer for Unsupervised Domain Adaptation. In *Proc. ICML*, 2020. 2
- [14] Yuejiang Liu, Parth Kothari, Bastien van Delft, Baptiste Bellot-Gurlet, Taylor Mordan, and Alexandre Alahi. TTT++: When Does Self-Supervised Test-Time Training Fail or Thrive? In *NeurIPS*, 2021. 2, 3
- [15] Zhipeng Luo, Zhongang Cai, Changqing Zhou, Gongjie Zhang, Haiyu Zhao, Shuai Yi, Shijian Lu, Hongsheng Li, Shanghang Zhang, and Ziwei Liu. Unsupervised Domain Adaptive 3D Detection with Multi-Level Consistency. In *Proc. CVPR*, 2021. 2
- [16] M Jehanzeb Mirza, Jakub Micorek, Horst Possegger, and Horst Bischof. The Norm Must Go On: Dynamic Unsupervised Domain Adaptation by Normalization. In *Proc. CVPR*, 2022. 2, 3, 6
- [17] Yatian Pang, Wenxiao Wang, Francis EH Tay, Wei Liu, Yonghong Tian, and Li Yuan. Masked Autoencoders for Point Cloud Self-supervised Learning. *arXiv preprint arXiv:2203.06604*, 2022. 1, 2, 3, 4, 5, 9
- [18] Can Qin, Haoxuan You, Lichen Wang, C-C Jay Kuo, and Yun Fu. PointDAN: A Multi-Scale 3D Domain Adaption Network for Point Cloud Representation. *NeurIPS*, 2019. 2
- [19] Jiawei Ren, Liang Pan, and Ziwei Liu. Benchmarking and Analyzing Point Cloud Classification under Corruptions. *Proc. ICML*, 2022. 1, 2
- [20] Yuefan Shen, Yanchao Yang, Mi Yan, He Wang, Youyi Zheng, and Leonidas J Guibas. Domain Adaptation on Point Clouds via Geometry-Aware Implicits. In *Proc. CVPR*, 2022. 2
- [21] Guangsheng Shi, Ruifeng Li, and Chao Ma. Pillarnet: Real-time and high-performance pillar-based 3d object detection. *arXiv preprint arXiv:2205.07403*, 2022. 8
- [22] Inkyu Shin, Yi-Hsuan Tsai, Bingbing Zhuang, Samuel Schulter, Buyu Liu, Sparsh Garg, In So Kweon, and Kuk-Jin Yoon. Mm-tta: Multi-modal test-time adaptation for 3d semantic segmentation. In *Proceedings of the IEEE/CVF Conference on Computer Vision and Pattern Recognition*, pages 16928–16937, 2022. 3
- [23] Baochen Sun and Kate Saenko. Deep CORAL: Correlation Alignment for Deep Domain Adaptation. In *Proc. ECCVW*, 2016. 2
- [24] Jiachen Sun, Qingzhao Zhang, Bhavya Kailkhura, Zhiding Yu, Chaowei Xiao, and Z Morley Mao. Benchmarking Robustness of 3D Point Cloud Recognition Against Common Corruptions. *arXiv preprint arXiv:2201.12296*, 2022. 5, 7
- [25] Yu Sun, Xiaolong Wang, Zhuang Liu, John Miller, Alexei Efros, and Moritz Hardt. Test-Time Training with Self-Supervision for Generalization under Distribution Shifts. In *Proc. ICML*, 2020. 2, 3, 5, 6, 7, 9
- [26] Mikaela Angelina Uy, Quang-Hieu Pham, Binh-Son Hua, Duc Thanh Nguyen, and Sai-Kit Yeung. Revisiting Point Cloud Classification: A New Benchmark Dataset and Classification Model on Real-World Data. In *Proc. ICCV*, 2019. 5
- [27] Pascal Vincent, Hugo Larochelle, Yoshua Bengio, and Pierre-Antoine Manzagol. Extracting and Composing Robust Features with Denoising Autoencoders. In *Proc. ICML*, 2008. 2
- [28] Dequan Wang, Evan Shelhamer, Shaoteng Liu, Bruno Olshausen, and Trevor Darrell. Tent: Fully Test-time Adaptation by Entropy Minimization. In *Proc. ICLR*, 2020. 2, 3
- [29] Qin Wang, Olga Fink, Luc Van Gool, and Dengxin Dai. Continual Test-Time Domain Adaptation. In *Proc. CVPR*, 2022. 3
- [30] Yan Wang, Xiangyu Chen, Yurong You, Li Erran Li, Bharath Hariharan, Mark Campbell, Kilian Q Weinberger, and Wei-Lun Chao. Train in Germany, Test in The USA: Making 3D Object Detectors Generalize. In *Proc. CVPR*, 2020. 2
- [31] Zhirong Wu, Shuran Song, Aditya Khosla, Fisher Yu, Linguang Zhang, Xiaoou Tang, and Jianxiong Xiao. 3D ShapeNets: A Deep Representation for Volumetric Shapes. In *Proc. CVPR*, 2015. 5
- [32] Li Yi, Boqing Gong, and Thomas Funkhouser. Complete & Label: A Domain Adaptation Approach to Semantic Segmentation of LiDAR Point Clouds. In *Proc. CVPR*, 2021. 2
- [33] Jure Zbontar, Li Jing, Ishan Misra, Yann LeCun, and Stéphane Deny. Barlow Twins: Self-Supervised Learning via Redundancy Reduction. In *Proc. ICML*, 2021. 2
- [34] Werner Zellinger, Thomas Grubinger, Edwin Lughofer, Thomas Natschläger, and Susanne Saminger-Platz. Central Moment Discrepancy (CMD) for Domain-Invariant Representation Learning. In *Proc. ICLR*, 2017. 2
- [35] Marvin Zhang, Sergey Levine, and Chelsea Finn. MEMO: Test Time Robustness via Adaptation and Augmentation. *arXiv preprint arXiv:2110.09506*, 2021. 2, 3